Assessing the potential of application of titanium dioxide for photocatalytic degradation of deposited soot on asphalt pavement surfaces

Assessing the Potential of Application of Titanium Dioxide for Photocatalytic Degradation of Deposited Soot on Asphalt Pavement Surfaces

Seyed Reza Omranian[1*], Michiel Geluykens[1], Myrthe Van Hal[2], Navid Hasheminejad[1], Iran Rocha Segundo[4,5], Georgios Pipintakos[1], Siegfried Denys[2], Tom Tytgat[2], Elisabete Fraga Freitas[4], Joaquim Carneiro[5], Sammy Verbruggen[2,3], Cedric Vuye[1]

[1]University of Antwerp, Faculty of Applied Engineering, EMIB Research Group, Groenenborgerlaan 171, B-2020 Antwerp, Belgium

[2]University of Antwerp, Faculty of Sciences, Sustainable Energy Air & Water Technology (DuEL), Groenenborgerlaan 171, B-2020 Antwerp, Belgium

[3]University of Antwerp, NANOlab Center of Excellence, Groenenborgerlaan 171, 2020 Antwerp, Belgium

[4]Institute for Sustainability and Innovation in Structural Engineering (ISISE), Department of Civil Engineering, University of Minho, 4800-058 Guimarães, Portugal

[5]Centre of Physics of Minho and Porto Universities (CF-UM-UP), Azurém Campus, University of Minho, 4800-058 Guimarães, Portugal

[*]Corresponding author Email address: SeyedReza.Omranian@uantwerpen.be

Abstract

It is known that pollutants and their irreparable influence can considerably jeopardize the environment and human health. Such disastrous, growing, hazardous particles urged researchers to find effective ways and diminish their destructive impacts and preserve our planet. This study evaluates the potential of incorporating Titanium Dioxide (TiO_2) semiconductor nanoparticles on asphalt pavements to degrade pollutants without compromising bitumen performance. Accordingly, the Response Surface Method (RSM) was employed to develop an experimental matrix based on the central composite design. Image Analysis (IA) was used to determine the rate of soot degradation (as pollutant representative) using MATLAB and ImageJ software. Confocal Laser Scanning Microscopy (CLSM), Fourier Transform Infrared spectroscopy (FTIR), and Dynamic Shear Rheometer (DSR) were finally carried out to estimate the effects of adding different percentages of TiO_2 on the microstructural features and dispersion of the TiO_2, chemical fingerprinting, and rheological performance of the bituminous binder. The results showed a promising potential of TiO_2 to degrade soot (over 50%) during the conducted experiments. In addition, the RSM outcomes showed that applying a higher amount of TiO_2 is more efficient for pollutant degradation. Finally, no negative impact was observed, neither on the rheological behavior nor on the aging susceptibility of the bitumen, even though the homogenous dispersion of the TiO_2 was clearly captured via CLSM.

Keywords: Photocatalytic Bituminous Pavement, Photocatalytic Semiconductor, Titanium Dioxide Nanoparticles, Response Surface Method, Soot Degradation, Image Analysis

1. Introduction

The World Health Organization (WHO, 2016) reported that approximately 91% of the world population lives in places with poor air quality conditions, where the level of pollutants exceeds the WHO air

quality guidelines, both in urban and rural regions [1]. It has been shown that exposure to pollutants can directly result in severe cardiovascular and respiratory diseases. Accordingly, various environmental deadlines have been proposed to tackle the negative impact of pollutants on human health and well-being, the environment, and their (in)direct influence on global warming. Several technologies have been developed to degrade pollutants into non-toxic substances. Among them, semiconductor-based photocatalysts have received considerable attention due to their capability to absorb and convert solar energy and degrade pollutants [2]. Several types of photocatalysts including zinc oxide (ZnO) [3], bismuth oxide (Bi_2O_3) [4], Graphitic carbon nitride (g-C_3N_4) [5], and tourmaline [6] have been utilized in the road industry to investigate their pollutant degrading capabilities. Nevertheless, TiO_2 gained more visibility due to its stability and low cost compared to other photocatalysts as well as its substantial benefits for self-cleaning, improved water evacuating intended for road safety, and heat/light-reflecting (pavement) surfaces to moderate Urban Heat Island [7-9].

The application of TiO_2 has also been occasionally investigated in road industries (real scales). The large road surface area (approximately 2% of the land) and their vicinity to the vehicle emissions turn asphalt pavements into an interesting platform to be functionalized for environmental remediation purposes by the degradation of air pollutants. Fan et al. (2017) reported successful removal of NO_x using carbon-modified TiO_2 (C-TiO_2) onto the asphalt surface. It was revealed that proper material preparation and optimization can result in effective, durable, and economical TiO_2 application [10]. In other studies, Rocha Segundo et al. (2018) confirmed by Rhodamine B (RhB) dye degradation, the TiO_2 potential to degrade organic pollutants when it was sprayed on the surface of asphalt mixtures [7]. Chen et al. (2021) compared different TiO_2 application methods on concrete pavements and discovered that the suspension-spraying method exhibited the best photocatalytic performance in terms of NO decomposition. It was also stated that future studies should be executed on materials suspension and their dispersion stability enhancement [11]. Moreover, it is important to consider all possible impacts on driving comfort and safety when any sort of modification is applied to the surface of a pavement. In this regard, skid resistance is particularly relevant, and has been studied in more detail by Rocha Segundo et al. (2019), where no significant impact was detected [12]. In addition, TiO_2 is a bright white material, and may therefore interfere with the visibility of road markings. It is also important to consider the durability of the application itself, as well as the potential release of hazardous particles to the environment since the road surface is submitted to heavy abrasion by vehicle tires [13, 14]. Although several studies have been conducted covering multiple application methods and dosages of TiO_2 in pavement technologies, no practical recommendation regarding TiO_2 application has yet been proposed.

Vehicular emission is considered one of the critical factors that contribute to urban pollution. According to Hwang et al. (2019), urban roads are contaminated by organic pollutants such as petroleum hydrocarbons (oils and fuels) and herbicides that are released from vehicles and/or road management practices [15]. Vehicles generate different amounts of pollutants depending on their engine, making it hard to measure the amount of soot formation. However, the trace of soot on the pavement was clearly observed through studies on road water runoff contamination and road dust [16, 17]. Deposition of pollutants in the form of soot due to the accumulation of cars' fuel combustion, particularly in areas with heavy traffic, can (in)directly influence the pavement roughness, the acidity of the rainfall-runoff, and contaminate soil and underground water [18-20]. This study attempts to evaluate the potential of TiO_2 incorporation in the pavement industry to degrade soot on the road surface. Accordingly, a comprehensive experimental matrix was first designed using the Response Surface Method (RSM). Produced specimens were then examined through elaborated laboratory testing procedures using Image Analysis (IA), Confocal Laser Scanning Microscopic (CLSM), Fourier Transform Infrared Microscopy (FTIR), and Dynamic Shear Rheometer (DSR) evaluation.

According to previous studies, RSM is a reliable technique to establish the relationships between independent (experimental) factors and dependent factors (responses) [22]. RSM has been effectively used in several research domains, including environment and pavement technologies. For instance, Haghshenas et al. (2020) used RSM to develop a new short-term aging protocol. In a similar study, Omranian et al. (2018) incorporated RSM to determine the optimal aging condition to enhance mixtures' fracture properties. Both studies reported RSM's potential to reliably understand and accurately predict changes in the responses [21, 22]. A recently published book entitled "Response Surface Methodology in Engineering Science" broadly presents modern RSM applications in different engineering fields [23].

Aside from RSM, Image Analysis (IA) has also gained popularity due to its substantial accuracy to differentiate between the changes in material characteristics in terms of brightness and colors compared to the relatively inferior human vision [24]. IA is typically used to process and analyze images either obtained from cameras or acquired by different microscopes. For instance, Stolte and Fang (2020) reported extensive incorporation of IA in the field of medical science and more particularly diagnosing diabetic retinopathy. It was reported that accurate IA can considerably outperform the sensitivity, detection, and grading of diabetic retinopathy compared to human observation [25]. IA was also utilized in the construction field. Hoong et al. (2020) reported that the composition of recycled aggregates can be determined by coupling IA and deep machine learning [26]. Hasheminejad et al. (2019) used IA on images captured by a camera to investigate crack propagation and proposed novel indices to assess the healing potential of asphalt mixtures [27]. Du et al. (2021) reviewed different IA applications from micro to macro scales in the field of pavement engineering. It has been reported that if the right devices are selected, IA can be a promising method for analyzing pavement materials [28].

Some of the most promising techniques to investigate the microstructure of bitumen are Atomic Force Microscopy (AFM), Environmental Scanning Electron Microscopy (ESEM), and Confocal Laser Scanning Microscopy (CLSM) [29]. Mirwald et al. (2022) recently published work on how AFM and CLSM can be employed to their maximum capabilities in order to acquire microstructural information through an investigation of five different bitumen microstructures. It was reported that although clear differentiation between the binders was difficult to attain, imaging analysis showed a satisfactory connection between both techniques [30]. It is worth mentioning that CLSM has especially gained more attention due to its ability to conduct fully non-contact measurements with nano-level resolution comparable to AFM [31, 32]. For instance, CLSM was recently used to observe the microstructure of bitumen at different aging stages and investigate their changes using deep learning and IA [33].

The main goal of this study was to determine the potential of nano-TiO_2 particles to degrade pollutants without compromising bitumen performance. Hence, aside from evaluating the potential of soot degradation applied on the surface of asphalt pavement, the impacts of TiO_2 on bitumen rheological and chemical composition were investigated, including the possible effect of exposure to UV light. Finally, a microscopic evaluation was performed on modified bitumen samples to investigate the distribution of TiO_2 on the surface and its influence on the microstructure of the bitumen. This paper begins with a brief literature review of previous related research both in terms of materials and technologies. Section two covers the material properties and sample preparation, testing procedures, and design of experimental procedures to assess TiO_2 efficiency and performance. The following section is built upon presenting and discussing the main results. The conclusions and recommendations/limitations are provided in the last section.

2. Materials and Methods

2.1. Materials

2.1.1. Nano-TiO_2

In this study, commercially available benchmark photocatalyst Evonik P25 TiO_2 was selected for incorporation in asphalt samples. The basic technical properties of the utilized TiO_2 are provided in Table 1, as reported by the supplier.

Table 1: Technical properties of Evonik P25 TiO_2

Parameters	Values
Appearance	White powder
Specific surface area (m^2/g)	35 – 65
Particle size (nm)	23 - 28
Loss on drying 105°C, 2h (%)	≤1.≤1.5
Purity (%)	≥ 99.5
pH-value, in 4% dispersion	3.5 – 4.5
Crystal form	80% Anatase, 20% Rutile

2.1.2. Asphalt bitumen and mixtures

Since this study aimed to evaluate the efficiency and impacts of TiO_2 on the degradation of soot as a pollutant, colored mixtures can exhibit better contrast to distinguish between the asphalt sample and dark soot particles. Accordingly, a red-colored loose asphalt mixture generally used for bicycle path surface layers was chosen. For this study, a dense-graded asphalt mixture, AC-6 (6-mm maximum nominal aggregate size) produced with 50/70 penetration grade bitumen (5.6% bitumen content), limestone aggregate, and filler which was colored with red dye (0.5% by the weight of the bitumen) was collected from Colas asphalt mixing plant in Wijnegem, Belgium. It should be noted that the same bitumen without red dye was used for modification procedures of bitumen with TiO_2.

2.2. Methods

Prior to explaining this section, the flowchart of this research is illustrated in Figure 1 for a better understanding of manuscript structure and flow.

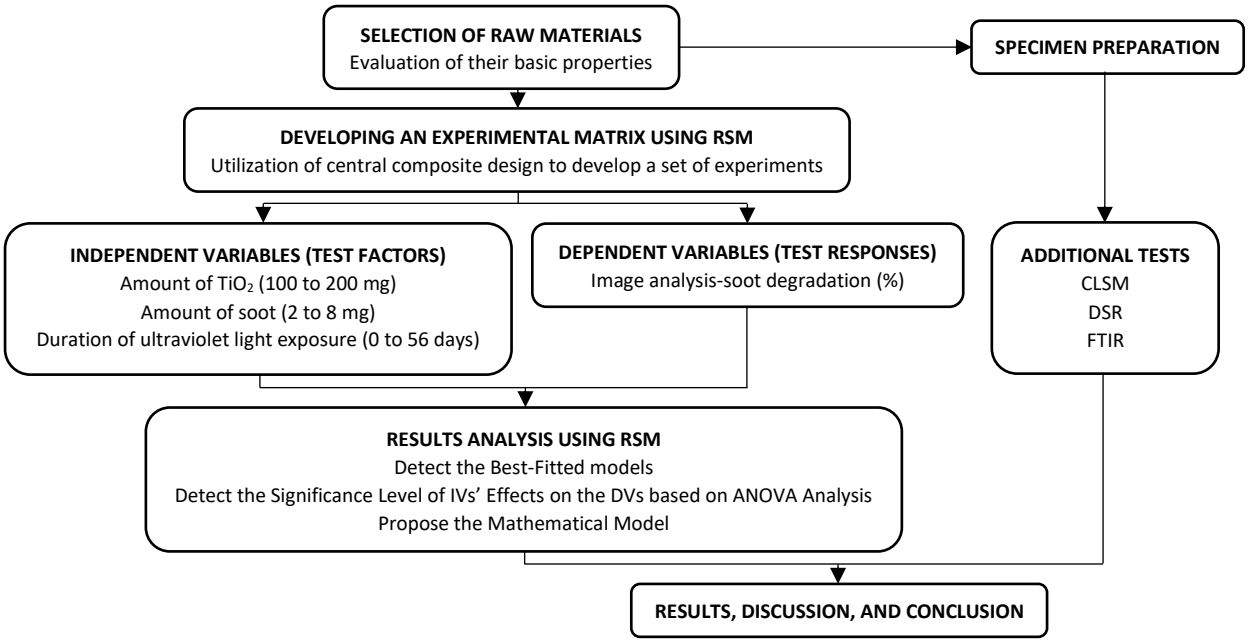

Figure 1: Research flowchart

2.2.1. Experimental design

RSM provides a Central Composite Design (CCD) method, one of the most popular approaches due to the lower number of required samples. This method was, therefore, used to design an experimental matrix. In this method, numerical factors vary based on the highest and lowest axial points as well as center points. Different amounts of Evonik P25 TiO_2 and soot were thus considered as independent variables (IVs), while the test outcomes were taken as dependent variables (DVs). It is worth mentioning that according to the designed matrix, three samples were prepared and tested at central point condition (for repeatability) to estimate the experimental error. Table 2 provides the experimental matrix designation based on various combinations of soot and TiO_2 quantities.

Table 2: Designated experimental matrix.

Sample	Designated	TiO_2 (mg)	Soot (mg)
S1	T100/S2	100	2
S2	T150/S2	150	2
S3	T200/S5	200	5
S4	T150/S5	150	5
S5	T200/S8	200	8
S6	T100/S8	100	8
S7	T150/S5	150	5
S8	T200/S2	200	2
S9	T150/S8	150	8
S10	T150/S5	150	5
S11	T100/S5	100	5

2.2.2. Sample preparation

A. Photocatalytic coating and soot application

The collected loose mixture was first compacted in the laboratory using plate compaction according to EN 12697-33:2019 and then cut into smaller cubical pieces (size 5 cm^3) for placing into the

conditioning chamber. Following the previous research [34], suspensions of different amounts of TiO_2 (according to the experimental matrix design) with 2 ml of methanol were prepared. In order to avoid agglomeration of the particles in the suspensions, they were conditioned in a sonication chamber for 1 hour. Afterward, 200 µl of suspended TiO_2 was drop-casted on top of the cut surfaces of the asphalt mixture resulting in a coverage of approximately 0,08 L/m² for each sample. The asphalt samples were then dried at room temperature for 2 hours and subsequently placed in an environmental chamber at 80°C for another 24 hours. Similar procedures were then adopted to apply the soot on top of the dried $TiO_2$to evaluate the efficiency of photocatalytic activity by the soot degradation.

B. Bitumen modification

To evaluate the impacts of TiO_2 on bitumen rheological and chemical properties, 0, 1, 3, and 5% TiO_2 (by weight of binder) were mixed at 170 ˚C (following the corresponding mixing temperature for the utilized bitumen) with the collected bitumen from the asphalt plant using a Low-Shear Mixer (350 RPM) for 30 minutes. These samples were poured into a custom-made silicone mold of 25×75 mm^2 with approximately 1 mm height and placed under UV-A light irradiation at 10 W/m² intensity for designated testing periods.

2.2.3. Soot degradation and imaging analysis

TiO_2 is a semiconductor with a specific band structure, which allows an electron to be promoted from the valence band to the conduction band when irradiated by light with sufficient energy (below a certain wavelength usually limited to UV light). This phenomenon is called 'activation' and results in a positively charged hole in the conduction band and a negatively charged electron in the valence band. These charge carriers can degrade organic components, such as soot, through a radical pathway with several subsequent intermediate compounds [2]. Ideally, the soot is completely degraded to CO_2, which in the generated quantities is less harmful compared to the initial compound. However, when not fully degraded, intermediary side products may have adverse effects on the environment. Nevertheless, existing literature found favorable results in this regard [34, 35]. In order to evaluate the soot degradation, a similar procedure to that performed by Van Hal et al. (2019) was adopted [34]. After the sample preparation, the asphalt cubes were placed in a custom-made UV-box with constant UV irradiation (wavelength of 350 to 400 nm) of 10 W/m², as shown in Figure 2A. The distance between the light and surface of samples was maintained at 20 mm to satisfy the UV intensity which was verified using an irradiance spectroradiometer type Avaspec-3648-USB2 from Avantes. Pictures were taken in a controlled-light PhotoBox (Figure 2B) that excludes external light and allows direct illumination. A Canon EOS 145 500D camera was positioned 18 cm above the samples and the digital images were taken in manual mode (ISO 200, aperture f8, and focal exposure 1:5) at maximal resolution (5184×3456 at 72 dpi). To gain insight into the soot degradation and the time required to observe the photocatalytic activities, images were taken and analyzed at 0, 1, 4, 7, 14, 28, and 56 days of UV irradiation as shown in Figure 2C. In addition, a picture was taken without any soot added on top on day 0 as a reference for each sample.

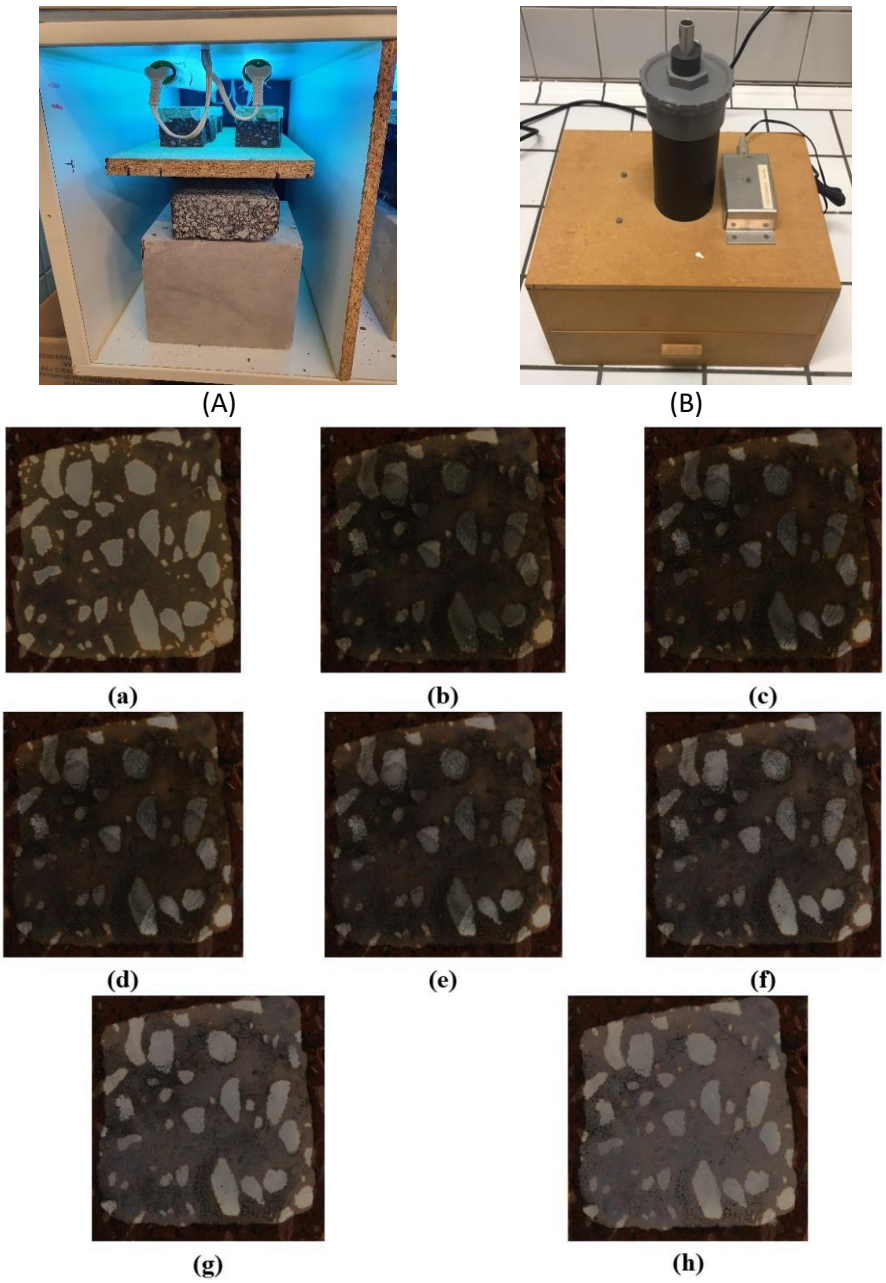

Figure 2: Utilized UV-irradiation setup (A), PhotoBox (B), and captured images at different degradation stages (C).

As a first attempt, the images were cropped to eliminate the irrelevant background and focus only on the specimens' surface. Determination of the amount of soot degradation was possible by converting the color images into greyscale due to the soot vanishing and visibility of the white TiO_2 surface after degradation. Every image was therefore analyzed using "MATLAB Image Processing Toolbox", following a MATLAB script to capture the greyscale values. To compare the changes in soot degradation, a histogram was then constructed by counting every pixel and plotting them in the corresponding 8-bit pixel value (0 = complete black; 255 = clear white). However, with this method, it proved difficult to quantify the soot degradation, as opposed to the original study by Van Hal et al. (2019) where this was easier as the substrate was a glass plate covered by a white catalyst layer, yielding a clearer grey contrast [34].

As a second attempt to validate the outcomes of the MATLAB Image Processing Toolbox and quantify the soot degradation, IA was also performed on grayscale cropped images using ImageJ software. The ImageJ computed the number of points that correspond to each of the segments. In this regard, the thresholding method was selected to classify and measure the different segments of the images. Prior to this step, the contrast of the images was slightly adjusted for better distinguishment of changes due to photocatalytic activities. The threshold values were then determined by a trial-and-error method. The images that were captured on the first day were used as a reference point to ensure the consistency and accuracy of the outcomes. Following the previous study, the overall accuracy level must be more than 85%. Otherwise, the entire classification process had to be repeated to determine the threshold range values [24].

2.2.4. RSM application

The relationship between IVs and the quantity of soot degradation (DV) was then determined using RSM. Different mathematical regressions, namely linear, quadratic, cubic, and two-factor interaction, were implemented to detect the most accurate regression model. Analysis of Variance (ANOVA) was carried out to establish the significance level of design factors and the impacts of their interactions. The best-fit model was selected according to the best results of lack-of-fit tests, and R^2 as well as F-tests and P-value, as shown by Prob>F, for further analysis. The F-tests and Prob>F (lower than 0.05) values indicate the significance level of the variance between the means of two populations and the probability of obtaining results as extreme as the observed data, respectively. Once the model was determined, a desirability index is defined based on the optimal rate of soot degradation. The target values were selected based on the minimum requirement for photocatalysis materials and the shortest period of UV exposure. This study utilized the Design-Expert 13 software to conduct the analysis.

2.2.5. Specimens characterization

In order to assess the impact of adding TiO_2 on the chemical composition, microstructural features, and rheological behavior of the binder, Confocal Laser Scanning Microscopy (CLSM), Fourier Transform Infrared Microscopy (FTIR), and Dynamic Shear Rheometer (DSR) were carried out.

A. CLSM

Prior to assessing specimens' performance, a CLSM test was conducted to guarantee homogenous dispersion of TiO_2. In this study, a Keyence CLSM with a VK-X1000 controller unit and a VK-X1050 measurement head coupled with two Nikon EPI Plan Apo 50X and 150X lenses (numerical apertures of 0.8 and 0.95, respectively) was used to investigate the microstructure of the modified bitumen. In ideal conditions, this microscope has a lateral resolution of 5 nm and an axial resolution of 10 nm. Two light sources are used in this microscope. Laser light with a wavelength of 661 nm scans the surface in the X, Y, and Z directions to capture the image containing the height information and white light to capture the color information from the sample surface. Moreover, a pinhole confocal optical system is used to eliminate all influences of ambient light and reflected light from any position other than the focal point. Microscopic images were acquired from the modified bitumen with four different TiO_2 percentages (0%, 1%, 3%, and 5%). Since the microstructural properties of bitumen are strongly dependent on the thermal history of the samples, the consistent preparation protocol proposed in [29] was used. This includes the following steps. To create a homogeneous workable material, 5 g of the binder was transferred inside a can and placed in a preheated oven set to 150°C for 5 minutes. Then, a sample holder (microscopy slide) was placed horizontally on a heating plate set at a temperature of 150°C. A drop of bitumen was placed on the sample holder and left for one minute

until a thin film with a flat surface was obtained. After removing the sample from the heating plate, it was placed inside a container (to prevent dust contamination) and left for 24 h to cool down to the ambient temperature. Then, three images at random locations were acquired from each sample using the microscope. Finally, the VK-MultiFileAnalyzer software and MATLAB were used to analyze the captured images.

B. DSR

Following EN 14770:2012 standard procedures, the frequency sweep test was carried out to evaluate the rheological behavior of the modified bitumen at two TiO_2 percentages (0% and 5%). In this study, an Anton Paar MCR 500 182 (Graz, Austria) DSR was employed to conduct the tests. DSR samples were produced for 8 mm and 25 mm geometries, and their performance was explored at two UV light exposure intervals (0 and 7 days). The test temperature was fluctuated from 0 to 40 °C for samples with 8 mm diameter (and 1 mm thickness) as well as 40 to 80 °C for samples with 25 mm diameter (and 2 mm thickness). The frequency sweep test was repeated at 10 °C elevated temperatures. Two replicates were carried out for the evaluation. The obtained data were analyzed using the RHEA™ software (v2.0, Abatech, Blooming Glen, PA, USA) to obtain the complex modulus and the Black space diagram.

C. FTIR

The Thermo Scientific Nicolet iS10 Fourier Transform Infrared spectrometer (Waltham, MA, USA), equipped with an Attenuated Total Reflectance (ATR) fixture and a Smart Orbit Sampling Accessory was employed to perform the tests. FTIR was carried out on modified specimens with four different TiO_2 percentages (0%, 1%, 3%, and 5%). Prior to the testing, all specimens were exposed to UV light irradiation for 0, 28, and 56 days to detect the likelihood of deviations in their chemical composition such as the presence of new peaks, the disappearance of peaks, or reduction/increase of chemical indices regarding the peak area contribution due to possible effects of UV-irradiation or TiO_2 on the aging of bituminous materials. At least four replicates were placed with the surface of the binder sample on the FTIR diamond to be analyzed. It should be mentioned that preliminary analyses on the contact between the prepared samples and the FTIR diamond were performed (trial and error) to guarantee sufficient accuracy of the outcomes. The average values after the acquisition of the spectra (32 repetitive scans in the range 400 cm^{-1} to 4000 cm^{-1} with a resolution of 4 cm^{-1}) were then recorded and analyzed.

3. Results and Discussion

3.1. Soot degradation and image analysis

3.1.1. Image processing using MATLAB

In total, soot degradation of 11 specimens with different soot and TiO_2 loadings was explored using MATLAB. Since all the specimens exhibited approximately similar trend lines (with different degradation rates), only the histogram for the extreme scenario (Table 2) which involved only 100 mg of TiO_2 to degrade 8 mg of soot is provided in this section. Figure 3 clearly shows the changes in the number of dark pixels representing soot coverage. It can be observed that the pinnacle of the number of soot pixels is higher than 120k px after application while the corresponding value drops to slightly below 40k px after 56 days of conditioning under UV light. Although some soot residue can still be spotted on the surface of the specimen, the clear potential of TiO_2 pollutant degradation on the surface of the pavement is visible. The results published by Van Hal et al. (2019) exhibited a similar trend with a higher soot degradation rate [34]. The difference can be correlated to the base materials

where soot was applied on glass slides instead of the complex, inconsistent, and rougher asphalt pavement surface. Since the developed MATLAB code was not able to clearly differentiate and compute the changes in the photocatalytic activities in terms of soot degradation, ImageJ software was incorporated for better quantification of the corresponding value (see Section 3.1.2).

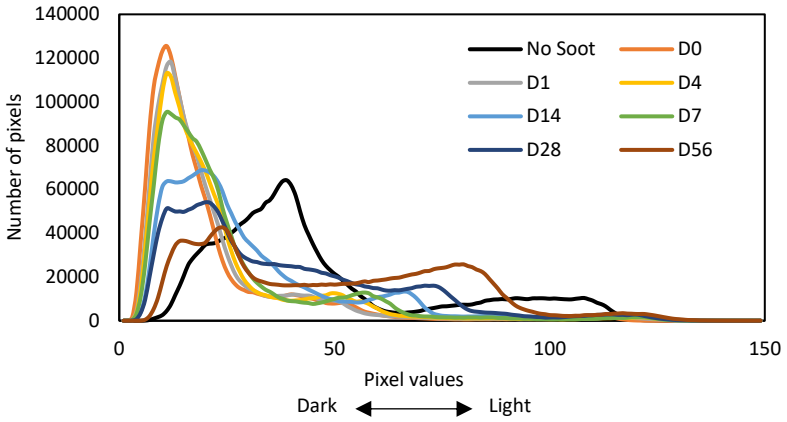

Figure 3: Histogram of sample T100/S8 (S6), where D is the conditioning days under UV light.

3.1.2. ImageJ and RSM outcomes

The soot degradation was quantified using ImageJ software, as results are provided in Table 3. The results were then analyzed using RSM as presented in Table 4 and Figures 4 to 7. From the set of tested models, the quadratic model was found to be the best model based on more reliable F-tests, lack-of-fit tests, and R^2 results, as shown in Table 4. It should be noted that the parameters with statistically insignificant influence on the model were omitted to enhance the accuracy and simplicity of the regression. The insignificance of Lack of Fit (higher than 5%) and acceptable R^2 and adjusted R^2 (approximately 90%) are indicative of the robustness of the developed model. Furthermore, the RSM's great capability and reliability in detecting the soot degradation with respect to the factors can be inferred from the even or normal distribution of residuals along the fitting lines. The plots of actual versus predicted results support this interpretation based on all predicted values from the provided equation in Table 4 fit into the experimental observations as shown in Figure 4.

Table 3: Soot coverage at different time intervals of UV exposure

Sample	Duration of UV light exposure (days)				
	1	7	14	28	56
S1	64.4%	57.3%	54.4%	31.7%	16.2%
S2	79.1%	69.6%	61.0%	51.1%	23.8%
S3	51.8%	39.8%	32.3%	29.0%	19.7%
S4	67.6%	62.2%	56.6%	41.2%	23.3%
S5	69.2%	63.3%	54.6%	42.9%	24.8%
S6	73.8%	70.5%	63.5%	55.8%	36.3%
S7	60.8%	52.4%	49.4%	36.3%	23.3%
S8	65.3%	58.1%	49.7%	19.1%	7.2%
S9	68.9%	60.4%	55.5%	50.9%	33.7%
S10	70.1%	65.2%	55.8%	41.3%	21.5%
S11	73.4%	69.0%	57.5%	43.2%	25.4%

Table 4: Proposed model and results of ANOVA analysis.

Source	Sum of Squares	DF	Mean Square	F-Value	Prob > F	Significant
Model	16101.89	12	1341.82	39.50	< 0.0001	Yes
A	914.11	1	914.11	26.91	< 0.0001	Yes
B	449.31	1	449.31	13.23	0.0007	Yes
C	13767.15	4	3441.79	101.33	< 0.0001	Yes
A^2	380.82	1	380.82	11.21	0.0017	Yes
B^2	424.18	1	424.18	12.49	0.0010	Yes
BC	335.47	4	83.87	2.47	0.050	Yes
Residual	1426.60	42	33.97			
Lack of Fit	1236.90	32	38.65	2.04	0.1166	No
R^2	0.919					
Adj R^2	0.895					

Soot Coverage = $48.95 - 5.52A + 3.87B + 18.62C_1 + 11.60C_2 + 4.56C_3 - 8.87C_4 - 3.37BC_1 - 2.34BC_2 - 2.44BC_3 + 4.08BC_4 - 5.48A^2 + 5.79B^2$

Note: DF is a degree of freedom, A represents the amount of TiO_2, B shows the amount of soot, and C stands for the period of UV-irradiation

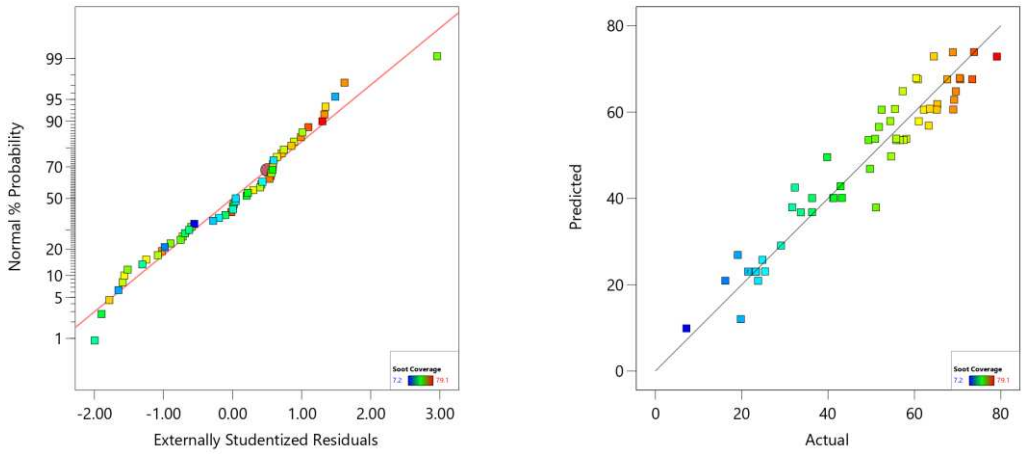

(a) (b)

Figure 4: Distribution of residuals (a), predicted VS experimental outcomes (b).

Figure 5 illustrates 3D contour plots showing the effects of the amount of soot and TiO_2 on the pollutant degradation rate at different UV exposure time intervals. The curvature of the amount of soot and TiO_2 presented in Figure 5a can be correlated to the inhomogeneous drop-casting application of the materials, despite the meticulous consistency of their amount, affecting the dispersion of the TiO_2 nanoparticles over the asphalt surface. In other words, the drop-casted materials stacked on top of each other resulted in curvatures, as can be seen in Figure 5a. According to Figure 5a, between 57 to 75% of the surface was covered by soot after day one, while the corresponding value is reduced to 26 to 55% and 9 to 38% after days 28 and 56, respectively. Steeper slopes of degradation curves show that increasing the amount of TiO_2 from 150 mg to 200 accelerates the soot degradation rate. Such a finding shows a better degradation potential of TiO_2 at a higher application proportion, particularly when a lower amount of soot is applied on the specimens. Figure 5 indicates that after less than two months, approximately 50% of the soot is degraded when the lowest amount of TiO_2 (100 mg) and the highest amount of soot (8 mg) were deposited on the specimens, while the corresponding value increased to more than 80% when the highest amount of TiO_2 and the lowest amount of soot were incorporated. These results clearly show the efficiency of functionalized asphalt mixtures with TiO_2 to photodegrade pollutants (confirming the photocatalysis activities) and its promising influence on the diminution of environmental concerns.

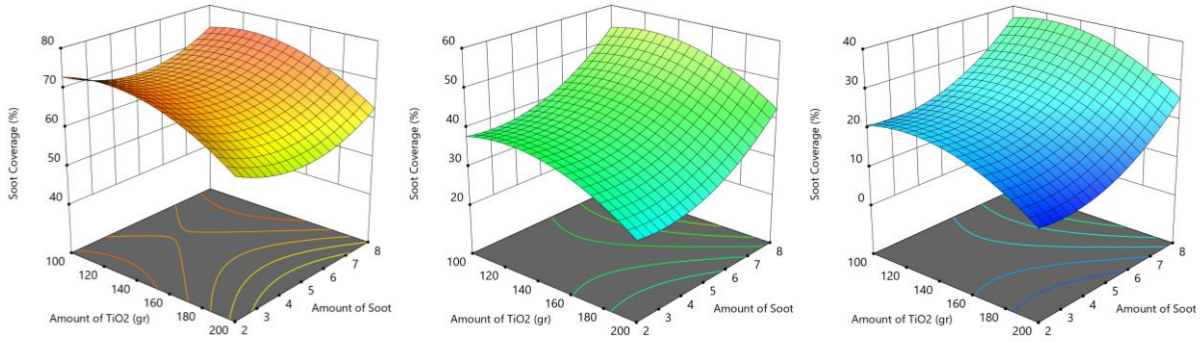

Day 1 (a) Day 28 (b) Day 56 (c)

Figure 5: Effects of different amounts of TiO_2 and soot.

For a better understanding of the changes in the rate of soot degradation Figure 6 presents the interaction between the influence of TiO_2 and soot deposition at different time intervals. The results indicate that the rate of soot degradation remains approximately unchanged during the first 14 days of UV light exposure for all specimens and the corresponding value accelerates from then on regardless of the amount of applied TiO_2. However, the increase in the amount of soot deposition slightly changes the degradation rate. From Figure 6, it can be seen that the degradation slope tends to remain unchanged until day 28, while this trend continues from this point with a steeper slope. Such a finding was expected since more time may be required for the reaction between TiO_2 and the upper layer (surface) of the thicker film of deposited soot.

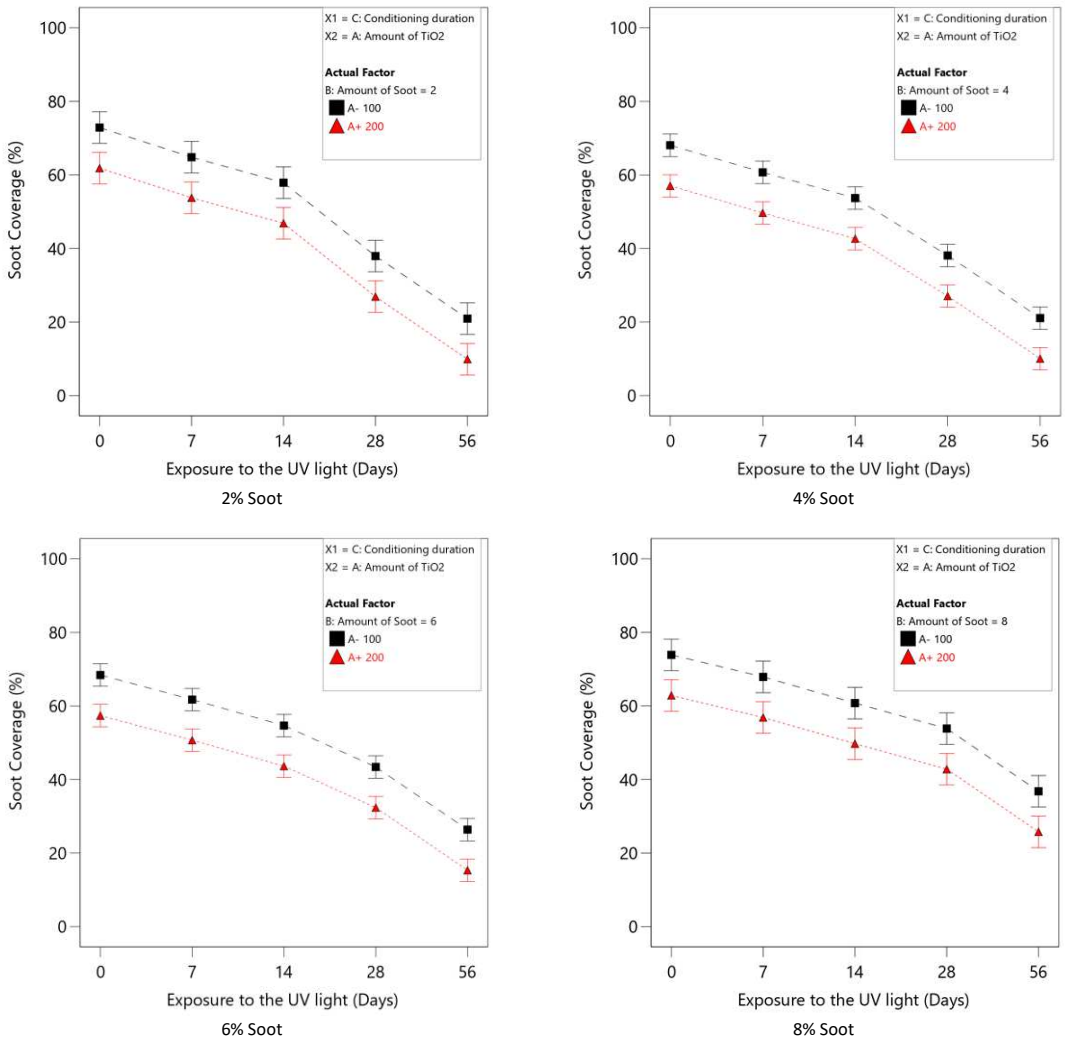

Figure 6: Interaction between the impact of the amount of soot and TiO_2 on degradation rate.

In order to determine the optimal combination scenario, the desirability index was calculated based on the shortest required period for maximum soot degradation with a lower amount of TiO_2 using RSM as the results presented in Figure 7. The findings indicate that the most efficient combination succeeded when the minimum amount of soot is deposited on the maximum amount of TiO_2 with desirability higher than 90%. It can also be seen that the slope tiptoed once the application rate of TiO_2 and soot exceeded the center points. It indicates that deposition of an extreme amount of either TiO_2 or soot may reduce their efficiency. Such findings may be associated with larger film thicknesses of soot or agglomeration of TiO_2 nanoparticles reducing the irradiation of the photocatalytic activities and consequently jeopardizing their effective chemical reactions.

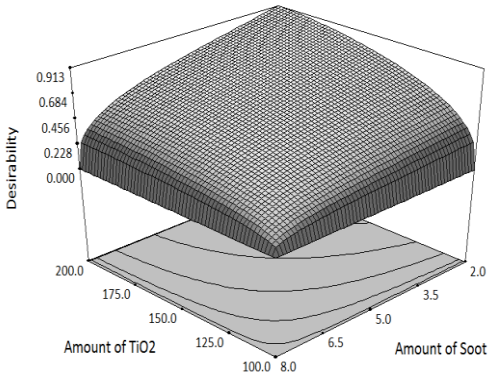

Figure 7: Desirability of the optimal amount of TiO_2 and soot application.

3.2. CLSM

The microstructure of the original and modified bitumen with different percentages of TiO_2 is investigated in this section. The processing of the images with VK-MultiFileAnalyzer included a reference plane setting to level the surface and a surface shape correction using waveform removal with a correction strength of 5 to remove the curvature of the bitumen drop. The height measurements on one location of each bitumen drop are illustrated in Figure 8. As presented in Figure 8a, the unmodified bitumen had a featureless microstructure which is consistent with the microstructure of non-waxy bitumen observed in the literature [36]. The influence of TiO_2 particles can be seen with the growth of peaks and valleys on the surface of the bitumen as the TiO_2 content increases. This figure also shows that the TiO_2 is distributed evenly in the bitumen and that no clustering can be spotted after the preparation procedures.

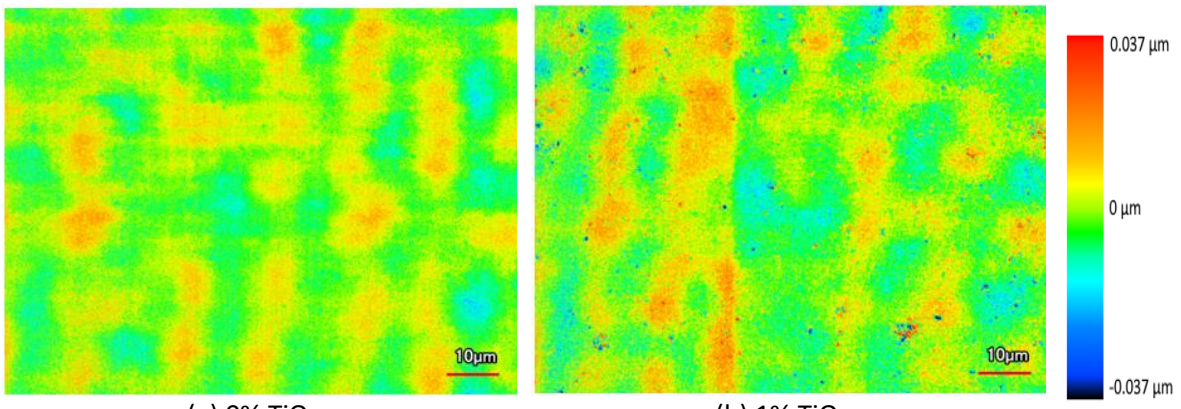

(a) 0% TiO_2 (b) 1% TiO_2

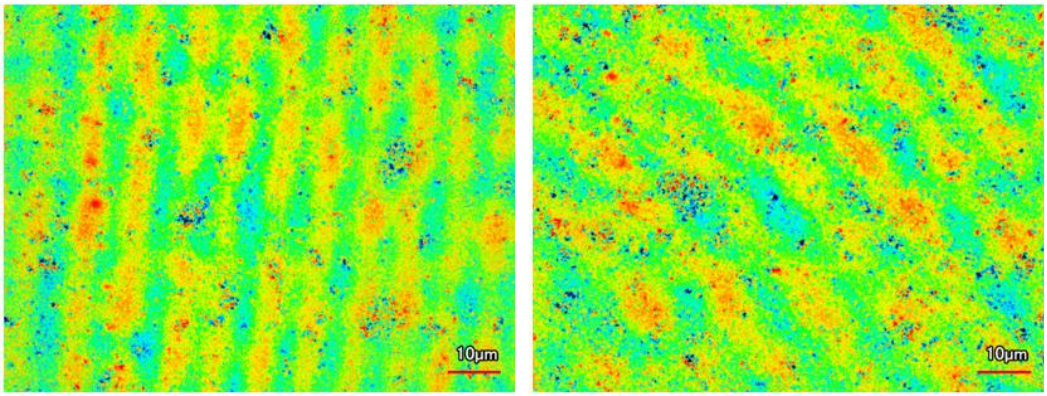

(c) 3% TiO_2 (d) 5% TiO_2

Figure 8: CLSM Height measurements on the surface of the bitumen containing different percentages of TiO_2.

To quantify the effect of TiO_2 content on the microstructure of the bitumen, measurements are conducted at three random rectangles on the surface of each sample with dimensions of about 92 µm by 69 µm. The arithmetical mean height (S_a), which indicates the average of the absolute value along the sampling length, and the percentage of the surface covered by peaks and valleys (P_{pv}), are calculated for each of these areas. The average values of these parameters and their standard deviations are presented in Figure 9. It can be seen that both S_a and P_{pv} increase with the rise in TiO_2 content. However, the standard deviation of both parameters remains very low for all percentages, indicating the even distribution of the TiO_2 on the surface of the samples.

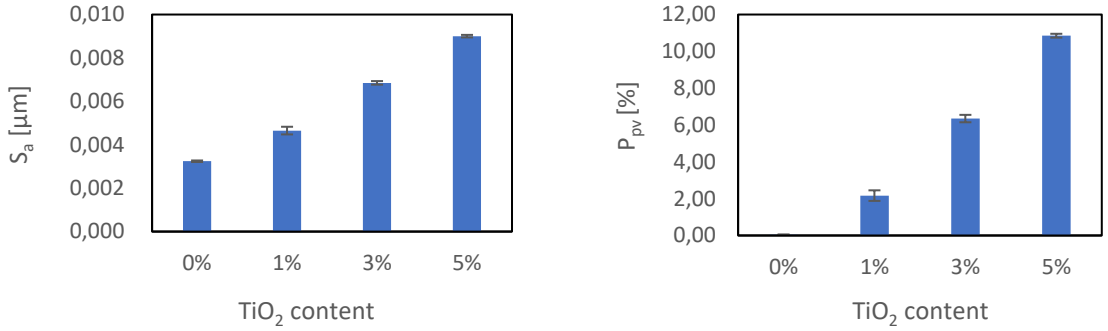

(a) (b)

Figure 9: Average arithmetical mean height (S_a) and the percentage of the surface covered by peaks and valleys (P_{pv}) for three images and their standard deviations

3.3. DSR

The potential influence of TiO_2 on bitumen's rheological characteristics was also evaluated. The results of the DSR tests are shown in Figures 10a and 10b in terms of the master curve and Black space diagram, respectively. As mentioned earlier, the impacts of two different percentages of TiO_2 (0% and 5%) on bitumen rheological behavior were evaluated at two different time intervals (0 and 7 days of UV irradiation). The results follow a typical pattern for bituminous binders despite the TiO_2 incorporation observing the highest G^* and lowest δ in the high-frequency domain. From Figure 10 (a or b), the G^* merely changes when bitumen is modified by 5% TiO_2. It can also be seen that the effects of aging imposed by UV exposure for 7 days were negligible since the complex modulus remained almost unchanged. Although no substantial effect of UV-aging was observed on the bitumen performance (similar to the study conducted by Zhang et al. (2021)), a more in-depth investigation might be necessary since Mirwald et al. (2022) reported significant impacts with different wavelengths

of UV irradiation and visible light on bitumen oxidation [37, 38]. This slight difference can be correlated to the incorporation of different methods of specimen fabrication and intensities (and wavelength) of UV light exposure. Similar to a typical Black space diagram of conventional bitumen, Figure 10b indicates that an increase in phase angle reduces complex modulus as illustrated in the Black Space Diagram. Nevertheless, Figure 10 exhibits no considerable impacts of TiO_2 or UV light on bitumen viscoelastic behavior. This finding is in line with the manuscript published by Rocha Segundo et al. (2020), where no evidence of variations was reported in the viscoelastic performance of a transparent binder modified up to 10% TiO_2 [39]. From these resemblance trends, it can be inferred that the utilized percentages of TiO_2 may not drastically change the viscoelasticity of the bitumen matrix based on their limited effects on bitumen performance. Furthermore, the effect of UV aging (after 7 days of exposure) may be negligible due to the relatively higher thickness of a DSR sample (1mm) compared to the TIO2 particles and their subsurface activation area. However, as mentioned earlier, a more in-depth research is required to broaden insight into the impacts of TiO_2 incorporation in bitumen in terms of aging, Physico-chemical, and rheological properties.

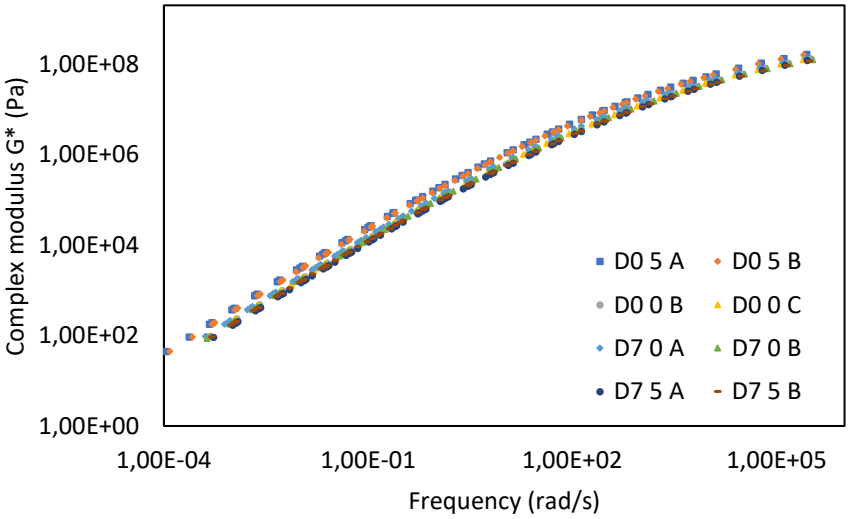

(a)

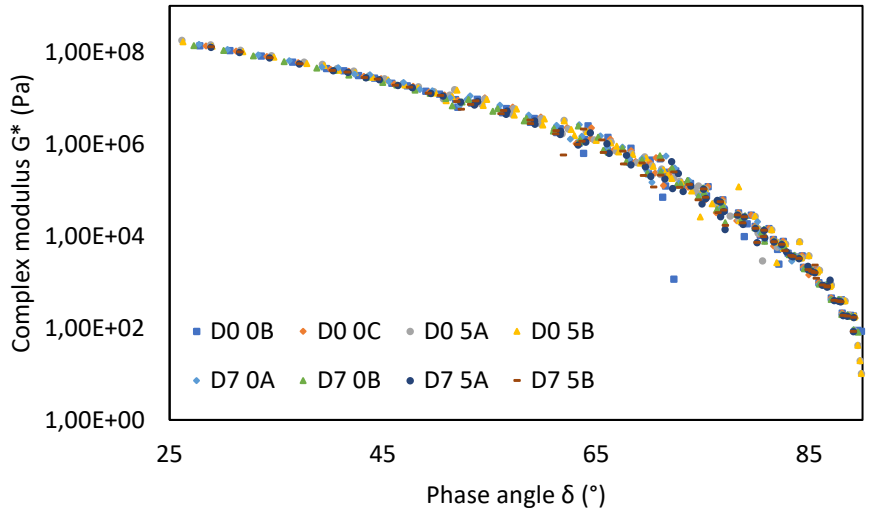

(b)

Figure 10: Master curve (a) and Black space diagram (b) of the modified binder with 0 and 5% TiO_2 at 0 and 7 days of UV exposure.

3.4. FTIR

Figure 11a presents the changes in FTIR spectra when different amounts of TiO_2 were incorporated at 0 days of UV exposure. Integration of certain functional groups can reveal information not only for the effect of UV but also for the percentage of TiO_2 presence in the composition of the bitumen. The procedure for the normalization of the spectra and integration of the areas around important functional groups as suggested in previous studies [40, 41] was adopted in this study. More specifically, for the integration mode, a two-step normalization was followed; namely a shift to zero absorbance at a fixed wavenumber of the lowest absorbance and then scaling of the total spectrum based on a ratio factor at the asymmetric stretching vibration of aliphatic structures at 2923 cm^{-1}.

The functional group of Ti-O bond in lower wavelengths of 434 cm^{-1} can be associated with the presence of TiO_2 as well as the peaks around 657 cm^{-1} and 590 cm^{-1} can be attributed respectively to Ti-O-Ti and Ti-O-O. Therefore integration of the area with integration limits between 400 and 667 cm^{-1} was used as a tracer of the utilized nano-modifier. Figure 11b clearly depicts this hypothesized relationship as this area is linearly increasing with higher TiO_2 percentages at 0 days of UV. Such trends show the FTIR capability to track the presence of TiO_2 in the bitumen. The effect of UV light in this area was also negligible, hence, it can be inferred that UV light will not influence the TiO_2 amount but rather the bitumen matrix.

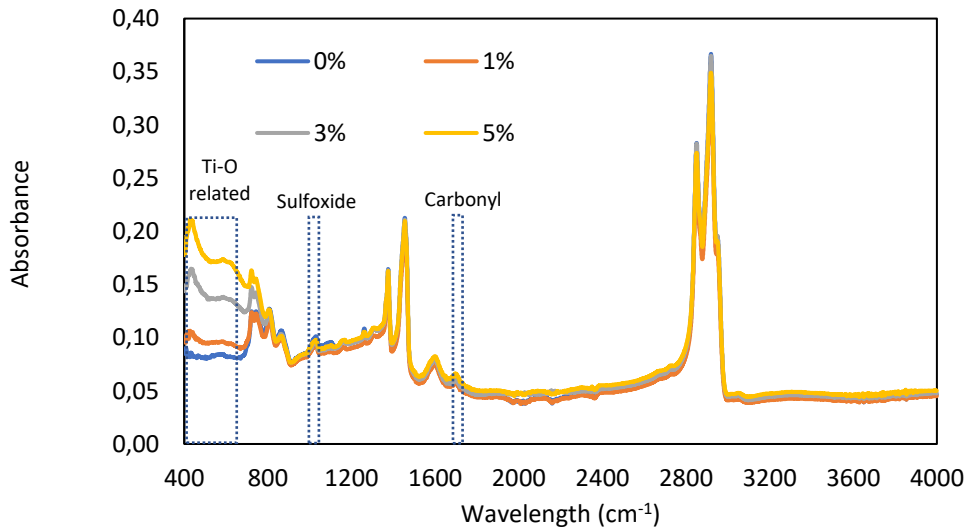

(a)

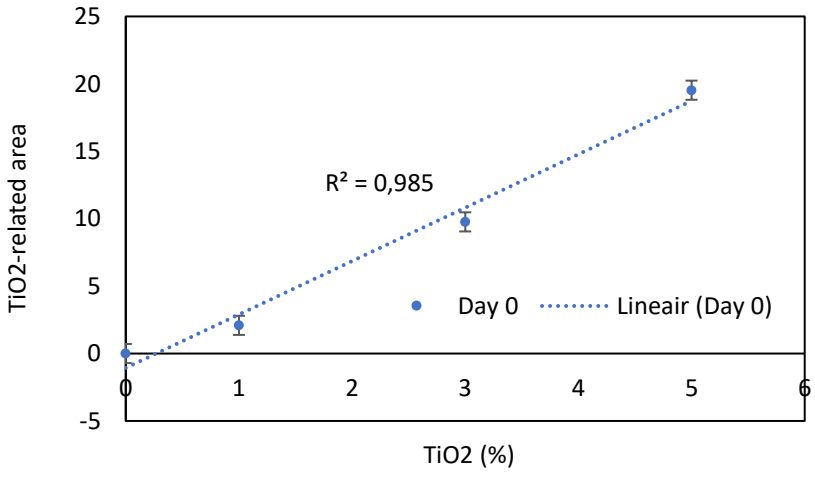

(b)

Figure 11: FTIR spectra and TiO_2-related functional groups with different percentages.

To further understand the possible aging impact of UV light, the results were analyzed in terms of carbonyl (ICO) and sulfoxide (ISO) indices as shown in Figures 12a and b, respectively. ICO and ISO are aging indicators of bituminous materials situated between wavelengths 1655-1760 cm^{-1} and 986-1047 cm^{-1}, respectively. The areas under the FTIR curve for ICO and ISO of all tested specimens are approximately 4±1% and 7±1%, respectively. Although a small increase in ISO for up to 3% TiO_2 with longer time intervals under UV can be observed, it seems that incorporation of higher percentages may even have a positive impact on the binder's surface oxidation. On the other hand, the ICO seems to follow a similar trend for the higher presence of TiO_2, whereas the differences with increasing UV are less pronounced as can be seen in Figure 12a. Thus, the current findings indicate inferior UV influence on the aging of bitumen a fact that is highlighted more with extended UV duration and lower TiO_2. Nevertheless, the extent of differences of the aging indices is considered small in the range of UV-A light (315-400 nm) as compared with changes observed in a recent study conducted by Mirwald et al. (2022) [38]. Eventually, it can be concluded that incorporating TiO_2 and specimens' exposure to UV light may have a small positive impact on the severity of oxygenated functional groups in bitumen.

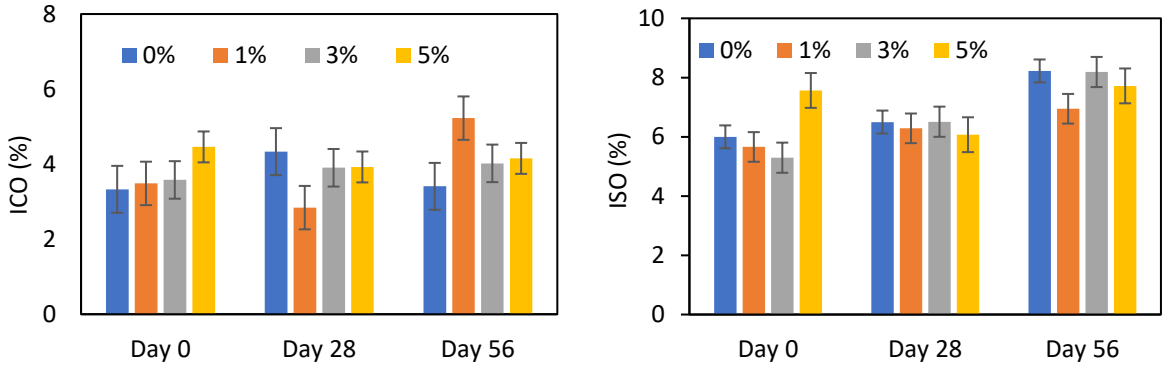

(a) (b)

Figure 12: ICO (a) and ISO (b) and their evolution with UV exposure time.

4. Conclusions

This study evaluated the potential of pollutant photodegradation by functionalized asphalt mixture with nanoparticles of TiO_2. The conclusions are divided into two parts, soot degradation, and physiochemical properties, as provided below respectively:

The overall results display the clear potential of TiO_2 to degrade soot and its promising influence on diminishing environmental concerns. IA conducted with both MATLAB and ImageJ software was found to be a reliable technique to precisely quantify the amount of soot degradation during the experimental procedures. Higher degradation efficiency was observed when the applied amount of TiO_2 was increased, particularly when a lower amount of soot was deposited on the specimens. This finding was also recognized based on the desirability measures obtained from RSM. In addition, when a lower amount of soot was applied on the surface, the degradation rate remains constant for the first 14 days of UV light exposure and starts to accelerate from this time forth, while the acceleration point is postponed until day 28 when a higher amount of soot was deposited on the specimens. Such outcomes indicate longer time requirements for the reaction between TiO_2 and the upper layer (surface) of the thicker film of deposited soot. The great accuracy of the developed model exhibited RSM's substantial capability to predict the soot degradation with respect to the input variables.

The morphological characterization of the specimens was also instigated and the analysis with the CLSM demonstrated that the TiO_2 (between 1 to 5%) is evenly distributed on the surface of the

material, and the increase in its amount can be observed on the surface microstructure of the samples. Furthermore, the possible impacts of TiO_2 on the binder were explored and the results proved that TiO_2 may neither negatively nor positively influence the viscoelastic behavior of bitumen. Using the FTIR technique, it is possible to detect the changes in the amount of TiO_2 based on the fluctuation of absorbance corresponding to the TiO_2 wavelength. However, no significant influence of TiO_2 and UV light exposure was observed on the aging indicators (ISO and ICO). Currently, the impacts of TiO_2 on the bitumen aging subjected to various conditions are under investigation. It is believed that using FTIR and CLSM enables scientists to discover if the amount of TiO_2 can beneficiary moderate the aging impacts under different environmental conditions.

Disclosure statement

No potential conflict of interest was reported by the authors.

Acknowledgments

The authors would like to thank the Industrial Research Fund (IOF) of the University of Antwerp for funding the project PAPPoA "Photocatalytic Asphalt Pavements for the Port of Antwerp (PAPPoA): a feasibility study (Port of the future)." (project nr. 41859) and AQ²UABIT "Advanced Qualitative and QUantitative surface Analysis of BITuminous binders using laser scanning confocal microscopy." (project nr. 40204). The authors from Portugal would like to acknowledge the Portuguese Foundation for Science and Technology (FCT) for funding the projects NanoAir PTDC/FISMAC/6606/2020, UIDB/04650/2020, and UIDB/04029/2020. Moreover, we would like to acknowledge as well master student Arne Chantrain for his effort throughout this study and excellent master thesis and Colas asphalt mixing plant for supplying the loose mixtures.

References

[1] World Health Organization. (2016). World health statistics 2016: monitoring health for the SDGs, sustainable development goals. World Health Organization. https://apps.who.int/iris/handle/10665/206498.

[2] Verbruggen, S. W. (2015). TiO2 photocatalysis for the degradation of pollutants in gas phase: From morphological design to plasmonic enhancement. Journal of Photochemistry and Photobiology C: Photochemistry Reviews, 24, 64-82.

[3] Le Pivert, M., Kerivel, O., Zerelli, B. & Leprince-Wang, Y. (2021). ZnO nanostructures based innovative photocatalytic road for air purification. Journal of Cleaner Production, 318, 128447.

[4] Yang, K., Li, R., Zhu, C. & Pei, J. (2021). Preparation, characterization and photocatalytic degradation efficacy of bismuth oxide under visible and ultraviolet light. Journal of Materials Research, 36, 2936-2949.

[5] Shan, B., Cao, X., Yang, X., Shang, T., Ding, Y. & Tang, B. (2021). Highly active photocatalytic asphalt pavement for NOx removal using iron-doped g-C_3N_4. Road Materials and Pavement Design, 1–16. https://doi.org/10.1080/14680629.2021.1984979.

[6] Wang, C., Li, Y., Sun, X. & Gao, Z. (2017). Automobile exhaust-purifying performance of tourmaline-modified asphalt concrete. Journal of Materials in Civil Engineering, 29, 04017004.

[7] Rocha Segundo, I., Ferreira, C., Freitas, E.F., Carneiro, J.O. Fernandes, F., Landi Júnior, S. & Costa, M.F. (2018). Assessment of photocatalytic, superhydrophobic and self-cleaning properties on hot mix

asphalts coated with TiO_2 and/or ZnO aqueous solutions. Construction and Building Materials, 166, 500-509.

[8] Zhong, Y. (2021). Research on Thermal Reflection and Cooling Curing Coating Material of Nano Modified Emulsified Asphalt for Urban Road Pavement. Proceedings of ICEMEE 2021 conference, Zhangjiajie, China. E3S Web of Conferences, 261, 02051.

[9] Jin, J., Xiao, T., Tan, Y., Zheng, J., Liu, R., Qian, G., ... & Zhang, J. (2018). Effects of TiO_2 pillared montmorillonite nanocomposites on the properties of asphalt with exhaust catalytic capacity. Journal of cleaner production, 205, 339-349.

[10] Fan, W., Chan, K. Y., Zhang, C., & Leung, M. K. (2017). Advanced solar photocatalytic asphalt for removal of vehicular NOx. Energy Procedia, 143, 811-816.

[11] Chen, C., Tang, B., Cao, X., Gu, F., & Huang, W. (2021). Enhanced photocatalytic decomposition of NO on portland cement concrete pavement using nano-TiO_2 suspension. Construction and Building Materials, 275, 122135.

[12] Rocha Segundo, I., Landi Jr, S., Oliveira, S., Freitas, E., Costa, M. F., & Carneiro, J. (2019). Photocatalytic asphalt mixtures: Semiconductors' impact in skid resistance and texture. Road Materials and Pavement Design, 20(sup2), S578-S589.

[13] Cordero, J. M., Hingorani, R., Jiménez-Relinque, E., Grande, M., Cutillas, F., Martinez, E., ... & Castellote, M. (2021). Challenges in quantification of photocatalytic NO2 abatement effectiveness under real world exposure conditions illustrated by a case study. Science of The Total Environment, 766, 144393.

[14] Nevshupa, R., Jimenez-Relinque, E., Grande, M., Martinez, E., & Castellote, M. (2020). Assessment of urban air pollution related to potential nanoparticle emission from photocatalytic pavements. Journal of Environmental Management, 272, 111059.

[15] Hwang, H. M., Fiala, M. J., Wade, T. L., & Park, D. (2019). Review of pollutants in urban road dust: Part II. Organic contaminants from vehicles and road management. International Journal of Urban Sciences, 23(4), 445-463.

[16] Zehetner, F., Rosenfellner, U., Mentler, A., & Gerzabek, M. H. (2009). Distribution of road salt residues, heavy metals and polycyclic aromatic hydrocarbons across a highway-forest interface. Water, Air, and Soil Pollution, 198(1), 125-132.

[17] Bandowe, B. A. M., Nkansah, M. A., Leimer, S., Fischer, D., Lammel, G., & Han, Y. (2019). Chemical (C, N, S, black carbon, soot and char) and stable carbon isotope composition of street dusts from a major West African metropolis: Implications for source apportionment and exposure. Science of the Total Environment, 655, 1468-1478.

[18] Khan, M., Qiao, F., & Yu, L. (2017). Wavelet analysis to characterize the dependency of vehicular emissions on road roughness. Transportation Research Record, 2641(1), 111-125.

[19] Arabani, M., Ranjbar Pirbasti, Z., & Hamedi, G. H. (2020). Evaluation of the Effect of Dust and Soot on Runoff Acidity and Moisture Sensitivity of Asphalt Mixtures Using Thermodynamic and Mechanical Methods. Journal of Materials in Civil Engineering, 32(11), 04020313.

[20] Indris, S. N., Rudolph, D. L., Glass, B. K., & Cappellen, P. V. (2020). Evaluating phosphorous from vehicular emissions as a potential source of contamination to ground and surface water. Cogent Environmental Science, 6(1), 1794702.

[21] Haghshenas, H. F., Rea, R., Byre, D., Haghshenas, D. F., Reinke, G., & Zaumanis, M. (2020). Asphalt binder laboratory short-term aging: Effective parameters and new protocol for testing. Journal of Materials in Civil Engineering, 32(1), 04019327.

[22] Omranian, S. R., Hamzah, M. O., Valentin, J., & Hasan, M. R. M. (2018). Determination of optimal mix from the standpoint of short term aging based on asphalt mixture fracture properties using response surface method. Construction and Building Materials, 179, 35-48.

[23] Kayaroganam, P. (2021). Response Surface Methodology in Engineering Science. Edited by Kayaroganam Palanikumar, Intechopen, DOI: 10.5772/intechopen.90965.

[24] Omranian, S. R., Hamzah, M. O., Yee, T. S., & Mohd Hasan, M. R. (2020). Effects of short-term ageing scenarios on asphalt mixtures' fracture properties using imaging technique and response surface method. International Journal of Pavement Engineering, 21(11), 1374-1392.

[25] Stolte, S., & Fang, R. (2020). A survey on medical image analysis in diabetic retinopathy. Medical image analysis, 64, 101742.

[26] Hoong, J. D. L. H., Lux, J., Mahieux, P. Y., Turcry, P., & Ait-Mokhtar, A. (2020). Determination of the composition of recycled aggregates using a deep learning-based image analysis. Automation in Construction, 116, 103204.

[27] Hasheminejad, N., Vuye, C., Margaritis, A., Ribbens, B., Jacobs, G., Blom, J., Van den bergh, W., Dirckx, J., Vanlanduit, S. (2019). Investigation of crack propagation and healing of asphalt concrete using digital image correlation. Applied Sciences, 9(12), 2459.

[28] Du, Z., Yuan, J., Zhou, Q., Hettiarachchi, C., & Xiao, F. (2021). Laboratory application of imaging technology on pavement material analysis in multiple scales: A review. Construction and Building Materials, 304, 124619.

[29] Pipintakos, G., Hasheminejad, N., Lommaert, C., Bocharova, A., & Blom, J. (2021). Application of Atomic Force (AFM), Environmental Scanning Electron (ESEM) and Confocal Laser Scanning Microscopy (CLSM) in bitumen: A review of the ageing effect. Micron, 103083.

[30] Mirwald, J., Hofko, B., Pipintakos, G., Blom, J., & Soenen, H. (2022). Comparison of Microscopic Techniques to study the Diversity of the Bitumen Microstructure. Micron, 103294.

[31] Pipintakos, G., Blom, J., Soenen, H., & Van den bergh, W. (2021). Coupling AFM and CLSM to investigate the effect of ageing on the bee structures of bitumen. Micron, 151, 103149.

[32] Blom, J., Soenen, H., Van den Brande, N., & Van den bergh, W. (2021). New evidence on the origin of 'bee structures' on bitumen and oils, by atomic force microscopy (AFM) and confocal laser scanning microscopy (CLSM). Fuel, 303, 121265.

[33] Hasheminejad, N., Pipintakos, G., Vuye, C., De Kerf, T., Ghalandari, T., & Blom, J. (2021). Utilizing deep learning and advanced image processing techniques to investigate the microstructure of a waxy bitumen. Construction and Building Materials, 313, 125481.

[34] Van Hal, M., Verbruggen, S. W., Yang, X. Y., Lenaerts, S., & Tytgat, T. (2019). Image analysis and in situ FTIR as complementary detection tools for photocatalytic soot oxidation. Chemical Engineering Journal, 367, 269-277.

[35] Smits, M., kit Chan, C., Tytgat, T., Craeye, B., Costarramone, N., Lacombe, S., & Lenaerts, S. (2013). Photocatalytic degradation of soot deposition: Self-cleaning effect on titanium dioxide coated cementitious materials. Chemical Engineering Journal, 222, 411-418.

[36] Pipintakos, G., Soenen, H., Goderis, B., Blom, J., & Lu, X. (2022). Crystallinity of Bitumen via WAXD and DSC and Its Effect on the Surface Microstructure. Crystals, 12(6), 755.

[37] Zhang, L., Gao, X., Wang, W., Wang, H., & Zheng, K. (2021). Laboratory Evaluation of Rheological Properties of Asphalt Binder Modified by Nano-TiO_2/$CaCO_3$. Advances in Materials Science and Engineering, vol. 2021, Article ID 5522025, 13 pages, 2021. https://doi.org/10.1155/2021/5522025.

[38] Mirwald, J., Nura, D., Eberhardsteiner, L., & Hofko, B. (2022). Impact of UV–Vis light on the oxidation of bitumen in correlation to solar spectral irradiance data. Construction and Building Materials, 316, 125816.

[39] Rocha Segundo, I., Landi, S., Margaritis, A., Pipintakos, G., Freitas, E., Vuye, C., ... & Carneiro, J. (2020). Physicochemical and rheological properties of a transparent asphalt binder modified with nano-TiO_2. Nanomaterials, 10(11), 2152.

[40] Hofko, B., Alavi, M. Z., Grothe, H., Jones, D., & Harvey, J. (2017). Repeatability and sensitivity of FTIR ATR spectral analysis methods for bituminous binders. Materials and Structures, 50(3), 1-15.

[41] Margaritis, A., Soenen, H., Fransen, E., Pipintakos, G., Jacobs, G., & Blom, J. (2020). Identification of ageing state clusters of reclaimed asphalt binders using principal component analysis (PCA) and hierarchical cluster analysis (HCA) based on chemo-rheological parameters. Construction and Building Materials, 244, 118276.